AJNR

Posttherapeutic Intraaxial Brain Tumor: The Value of Perfusion-sensitive Contrast-enhanced MR Imaging for Differentiating Tumor Recurrence from Nonneoplastic Contrast-enhancing Tissue

Takeshi Sugahara, Yukunori Korogi, Seiji Tomiguchi, Yoshinori Shigematsu, Ichiro Ikushima, Tomohiro Kira, Luxia Liang, Yukitaka Ushio and Mutsumasa Takahashi

AJNR Am J Neuroradiol 2000, 21 (5) 901-909
http://www.ajnr.org/content/21/5/901

AJNR Am J Neuroradiol 21:901–909, May 2000

Posttherapeutic Intraaxial Brain Tumor: The Value of Perfusion-sensitive Contrast-enhanced MR Imaging for Differentiating Tumor Recurrence from Nonneoplastic Contrast-enhancing Tissue

Takeshi Sugahara, Yukunori Korogi, Seiji Tomiguchi, Yoshinori Shigematsu, Ichiro Ikushima, Tomohiro Kira, Luxia Liang, Yukitaka Ushio, and Mutsumasa Takahashi

BACKGROUND AND PURPOSE: **Differentiation of tumor recurrence from treatment-related changes may be difficult with conventional MR imaging when newly enhancing lesions appear. Our aim was to determine the value of perfusion-sensitive contrast-enhanced MR imaging for differentiating recurrent neoplasm from nonneoplastic contrast-enhancing tissue.**

METHODS**: Twenty patients in whom new enhancing lesions developed within irradiated regions were examined prospectively with perfusion-sensitive contrast-enhanced MR imaging. Twelve of them also underwent thallous chloride Tl 201 single-photon emission tomography (^{201}Tl-SPECT). Normalized relative cerebral blood volume (rCBV) ratios and thallium indexes were evaluated to determine whether the new enhancing lesions were recurrent or not. Five instances of tumor recurrence and one of radiation necrosis were verified histologically; in the others, tumor recurrence was distinguished by lesions that progressively increased in size on serial MR examinations over at least 5 months, and nonneoplastic contrast-enhancing tissue was distinguished by lesions that disappeared or decreased in size on serial MR studies over at least 9 months.**

RESULTS: **When normalized rCBV ratios were higher than 2.6 or lower than 0.6, enhancing lesions were either recurrent (n = 5) or nonneoplastic contrast-enhancing tissue (n = 3), respectively. All nonneoplastic contrast-enhancing tissue had a low thallium index, whereas three of four recurrent lesions had a high index.**

CONCLUSION: **An enhancing lesion with a normalized rCBV ratio higher than 2.6 or lower than 0.6 may suggest tumor recurrence or nonneoplastic contrast-enhancing tissue, respectively. In these cases, further examination with ^{201}Tl-SPECT may not be necessary. However, when the normalized rCBV ratio is between 0.6 and 2.6, ^{201}Tl-SPECT may be useful in making the differentiation.**

Over the past several decades, therapy for patients with primary and metastatic CNS tumors has become more aggressive as neurosurgeons, neurooncologists, and radiation oncologists try to cure patients or at least provide them with a longer disease-free survival (1–3). Surgical resection and chemotherapy alone have proved to be insufficient in many instances. As a result, the various forms of radiotherapy, including high-dose external-beam radiation, radiosurgery, and radioactive seed implantation, have all become important therapeutic adjuncts. The end result is that radiation necrosis is being seen with increased frequency.

Serial MR examinations are used routinely in the assessment and surveillance of those patients. Features that are inspected for assessment of tumor progression are regions of abnormal contrast enhancement on postcontrast T1-weighted images and the volume of hyperintensity on T2-weighted images. Although such morphologic changes are indicative of the existence of the disease, it is often difficult to determine whether an enhanced lesion represents tumor recurrence or not, especially when the enhancement is initially observed (1, 3, 4). The lack of specificity has prompted investigation into other imaging techniques with the hope of finding a more reliable clinical tool.

Received March 3, 1999; accepted after revision November 22.

From the Departments of Radiology (T.S., Y.K., S.T., Y.S., I.I., T.K., L.L., M.T.) and Neurosurgery (Y.U.), Kumamoto University School of Medicine, Japan.

Address reprint requests to Takeshi Sugahara, MD, Department of Radiology, Kumamoto University School of Medicine, 1–1–1 Honjo, Kumamoto 860–8556, Japan.

Recently, functional MR imaging techniques have been significantly advanced through the extension of the anatomic capabilities of conventional MR imaging methods. Perfusion-sensitive contrast-enhanced MR imaging, which has made it possible to obtain measurements of vascularity within brain lesions and can be acquired during the same session as conventional MR imaging, allows exact comparison of those results (5–10). The vascularity of malignant tumor differs dramatically from that of irradiated brain tissue, specifically radiation necrosis. Thus, tumor recurrence within irradiated lesions may be differentiated from regions of radiation necrosis with perfusion-sensitive contrast-enhanced MR imaging. Our aim was to determine the value of this technique in the characterization of newly developed, small, enhancing lesions within irradiated regions after the treatment of brain tumors.

Methods

Patient Population

Twenty patients (10 men and 10 women; mean age ± SD, 43 ± 19 years) were prospectively entered into the study over a 24-month period on the basis of the following criteria: previous treatment with conventional external-beam radiation therapy and systemic chemotherapy after surgical resection for intraaxial tumors; new development of small, enhancing lesions within the radiation field 6 to 94 months after radiation; and T2-weighted MR imaging findings of enhancing areas surrounded by hyperintense areas, consistent with tumor recurrence (11, 12). All patients underwent follow-up MR examinations in intervals of 2 months or less once the newly developed, small, enhancing lesions were observed. None of the patients received any therapy during the follow-up period.

Initial diagnoses in all patients were proved by examination of histologic specimens. Sixteen patients had astrocytic tumors with pathologic grades of II (n = 4), III (n = 7), or IV (n = 5). In the remaining four patients, lesions consisted of two malignant gangliogliomas, one germinoma, and one primitive neuroectodermal tumor.

The final determination between tumor recurrence and nonneoplastic contrast-enhancing tissue was decided either histologically or clinicoradiologically. Five cases of tumor recurrence and one of radiation necrosis were histologically verified by either surgical resection or stereotactic biopsy. In the remaining patients who did not undergo surgical intervention, the lesions were considered to be nonneoplastic contrast-enhancing tissue when the enhanced lesions disappeared or decreased in size on subsequent MR examination, or were present but unchanged on serial follow-up MR examinations for 9 months, accompanied by neurologic improvement during the follow-up period. When the enhancing lesions increased progressively in size on at least three serial MR examinations over 5 months or more, and the patient's clinical condition deteriorated progressively during that period, they were interpreted as tumor recurrence.

Perfusion-sensitive contrast-enhanced MR images as well as conventional MR studies were obtained in all patients, and ^{201}Tl-SPECT examinations were obtained in 12 of them. The perfusion-sensitive contrast-enhanced studies and the ^{201}Tl-SPECT studies were performed an average of 29 months (range, 6–94 months) and 32 months (range, 7–98 months) after radiation therapy, respectively. The interval between perfusion-sensitive contrast-enhanced MR imaging and ^{201}Tl-SPECT ranged from 6 to 47 days (mean, 24 days).

Imaging Procedures

All MR images were obtained with a 1.5-T superconducting system. Conventional and perfusion-sensitive contrast-enhanced MR images were acquired during the same procedure to allow exact comparison of the results. Sagittal T1-weighted localizing images (15/6/1[TR/TE/excitations]) were acquired first, and then unenhanced axial T1-(690/14/1) and T2-weighted images were obtained in each patient. All conventional sequences were obtained with a 5-mm section thickness and a 1-mm intersection gap. Before perfusion-sensitive contrast-enhanced MR imaging was performed, a 21-gauge intravenous (IV) needle was inserted and retained in the vein of the right antecubital fossa.

The perfusion-sensitive contrast-enhanced MR images were obtained with a gradient-echo echo-planar (GE-EPI) technique (2000/40) with a readout band width of 926 Hz per pixel and a maximum amplitude of 25 mT/m before, during, and after injection of each contrast agent (7). Lipid suppression was used to suppress the signals from the subcutaneous fat, which would be superimposed on the brain because of large chemical-shift artifacts seen with the GE-EPI technique. Five-to-nine-section studies were acquired to cover the entire enhanced area. Axial sections were selected from the unenhanced images for dynamic MR imaging. After injection of 0.05 mmol/kg of contrast medium to minimize the effect of T1 shortening from enhancing lesions, a 0.10 mmol/kg bolus of gadopentetate dimeglumine was injected via a mechanical pump (3 mL/s), followed by a 20-mL saline flush. In all patients, 30 images were obtained at each section location during 60-second periods separated by 2-second intervals. Each section was collected by using a section thickness of 5 mm, an intersection gap of 1 mm, a 256 × 128 matrix, and a 20 × 22- to 28-cm field of view. After data collection, the relative cerebral blood volume (rCBV) maps were derived on a voxel-by-voxel basis from the dynamic imaging sets.

The starting and ending points of the first-pass transit of contrast agent through the brain were identified by using the time-activity curve of the means of the signal magnitudes of the pixels covering the whole-brain tissue in the section. Before the starting point of the first-pass circulation (seen as a drop in signal), representative baseline points were selected and their average was calculated for each voxel as a baseline measure for signal intensity (S_0). On a voxel-by-voxel basis, signal intensity (S) was converted to changes in T2* relaxation rate ($\delta R2^*$) as follows: $\delta R2^* = -\ln (S/S_0)/TE$. Previous experiments and theoretical data have shown that $\delta R2^*$ is approximately linearly proportional to the concentration of contrast material in the tissue (13–15). The rCBV maps were generated by numerical integration of relative concentration ($\delta R2^*$) for the first-pass bolus through each voxel based on kinetic principles for nondiffusible tracers (16, 17). The imaging process required approximately 30 minutes to integrate the functional time course data.

^{201}Tl-SPECT studies were obtained in 12 of 20 cases, because at the beginning of this study, ^{201}Tl-SPECT was not routinely performed for differentiating tumor recurrence from nonneoplastic contrast-enhancing tissue. Patients were scanned 20 minutes after IV injection of 111 MBq of thallous chloride Tl 201, using a three-head rotating gamma camera (Prism 3000; Picker, Highland Heights, OH). The camera heads were equipped with low-energy high-resolution fan-beam collimators. Data were acquired in a step-and-shoot mode from 120 directions, at 360°, with a 64 × 64 matrix. The energy peak was set at 70 keV, with an energy window of 20%. All SPECT scans were reconstructed using a filtered backprojection algorithm with a ramp filter before postfiltering with a Butterworth filter (cutoff, 0.20 cycle/cm; order, 8). Each section thickness was 6.3 mm. Attenuation and scatter corrections were not performed. The acquisition time at each projection was 40 seconds, for a total collection time of 20 minutes.

Image Evaluation

To calculate the normalized rCBV ratios (rCBV[tumor]/rCBV[contralateral tissue]), the regions of interest (ROIs) consisting of more than 20 pixels were located in the enhanced areas on the contrast-enhanced T1-weighted images and in the contralateral white matter, which was judged as normal on both T2- and contrast-enhanced T1-weighted images. Whenever possible, the ROI of normal white matter was placed contralateral to the ROI of tumor in the same transaxial plane. When this was not possible, the ROI was positioned in representative normal white matter in the same transaxial plane. To avoid the risk of calculating the rCBV from normal vessels, such as cerebral arteries and veins, the radiologist initially investigated the serial δR2* maps from arterial to venous phases as well as the conventional MR images and then located the ROIs within tumors. The δR2* maps clearly showed the rCBV from cerebral arteries or veins, and the ROIs were easily defined without superimposition on those vessels (18).

^{201}Tl-SPECT studies were quantified in the following manner. The location of the tumor and normal brain tissues on the ^{201}Tl-SPECT transverse sections was determined by comparing transverse sections from conventional MR images. If a focus of abnormal activity was discernible in that location, an ROI was drawn to encompass it. If no focus of abnormal activity was perceived, an ROI was drawn in the vicinity of the enhanced area, using the conventional MR images as a guide. In all cases, care was taken to avoid inclusion of any scalp activity in the ROI. The total counts in the ROI were recorded. Counts were then sampled in a region of equal size positioned over the normal brain tissue. The ratios between the total counts in the tumor regions and total counts in the corresponding normal white matter were calculated. The thallium index was defined as the ratio generated from counts of enhanced areas divided by those of normal white matter.

Statistical Analysis

A unpaired Student's *t*-test was used to determine whether there was a difference in the normalized rCBV ratios and thallium indexes between the patients with and without tumor recurrence. A difference of $P < .05$ was considered statistically significant.

Results

The Table summarizes the findings in the 20 patients. The maximum diameter of the newly developed, small, enhancing lesions ranged from 5 to 35 mm (mean, 17 mm). Of the 14 tumors without histologic verification, five were diagnosed as recurrent and nine as nonneoplastic contrast-enhancing tissue by noninvasive outcome parameters. The recurrent and nonneoplastic contrast-enhancing tissue groups included 10 patients each. At recurrence, three tumors that had initially been treated as low-grade gliomas had changed to anaplastic glioma (n = 1) or glioblastoma (n = 2). Therefore, all recurrent tumors, except for one primitive neuroectodermal tumor, were anaplastic gliomas or glioblastomas.

Newly enhancing lesions with a normalized rCBV ratio above 2.6 represented recurrent tumor (n = 5) (Fig 1). Two patients with these tumors also underwent ^{201}Tl-SPECT examination, which showed high uptake, consistent with tumor recurrence (thallium index, 3.22 and 7.70, respectively). The remaining five patients with tumor recurrence had normalized rCBV ratios less than 2.6. Three of four of these tumors examined with ^{201}Tl-SPECT showed high uptake (thallium index, >1.83), consistent with tumor recurrence (Fig 2).

A normalized rCBV ratio of less than 0.6 was observed only in patients with nonneoplastic contrast-enhancing tissue (n = 3) (Fig 3). Two of these patients also underwent ^{201}Tl-SPECT, which did not show any high uptake, consistent with a lack of tumor recurrence. The remaining seven patients with nonneoplastic contrast-enhancing tissue had normalized rCBV ratios higher than 0.6 (Fig 4). Four of these patients were examined with ^{201}Tl-SPECT, which did not show any abnormally high uptake, consistent with nonneoplastic tissue (Fig 5).

The relationship between normalized rCBV ratios and thallium indexes for tumor recurrence and nonneoplastic contrast-enhancing tissue is shown in Figures 6 and 7. Both the normalized rCBV ratios and thallium indexes of the tumor recurrence group were higher than those of the nonneoplastic group. The differences between the two groups reached statistical significance ($P = .03$ and 0.02, respectively).

Discussion

Ionizing radiation to the CNS may produce dramatic delayed postradiation damages after a delay of months from the time of radiation (19, 20). Those effects on the CNS consist mainly of radiation necrosis caused by blood-brain barrier disruption and diffuse white matter injury caused by radiation-induced demyelination (11, 21, 22). Radiation necrosis most commonly occurs at the site of the previous tumor, even after whole-brain radiation (21, 22). This predilection may be due to surrounding vasogenic edema, which may render the adjacent white matter more vulnerable to radiation damage (22). The MR imaging findings of radiation-induced brain damage include a ring-enhancing mass with variable edema and mass effect (21–24). These findings are often nonspecific and may not permit differentiation from tumor recurrence. Additionally, radiation-induced lesions occur within 2 years after radiation therapy, the same period during which tumor recurrence is most frequent (21, 22). In our series, most nonneoplastic lesions were consistent with radiation necrosis, although histologic verification was obtained only in one case.

Perfusion-sensitive contrast-enhanced MR imaging depicted tumor recurrence in approximately half the patients. The tumor growth consists of an irregular meshwork of vessels intermixed with normally existing vessels (2, 19, 20, 25, 26). These vessels markedly differ from those of radiation necrosis, which primarily consist of ischemic changes caused by the endothelial damage (27–30). Therefore, it is not surprising that in some cases perfusion-sensitive contrast-enhanced MR imaging, which is a technique that reflects histologic vas-

Results of a comparison between perfusion-sensitive MR imaging and ^{201}TI-SPECT

Case No.	Sex/Age (y)	Final Diagnosis	Primary Tumor	Time Since Initial Diagnosis (mo)	Radiation Dose (Gy)	Lesion Size (mm)	Normalized rCBV Ratio	Thallium Index
1	F/32	Recurrence*	Low-grade astrocytoma	94	60	14	0.64	1.83
2	M/78	Recurrence	Glioblastoma	12	60	33	0.83	3.29
3	F/35	Recurrence*	Low-grade astrocytoma	36	60	8	0.94	0.86
4	M/14	Recurrence*	PNET†	15	60	10	2.11	3.10
5	M/47	Recurrence*	Anaplastic astrocytoma	44	80	35	3.25	7.70
6	M/38	Recurrence	Anaplastic astrocytoma	53	60	25	4.45	3.22
7	M/45	Recurrence	Glioblastoma	6	60	22	3.08	…
8	F/54	Recurrence	Anaplastic astrocytoma	18	60	29	3.69	…
9	F/63	Recurrence*	Low-grade astrocytoma	62	60	10	4.45	…
10	F/64	Recurrence	Glioblastoma	11	60	20	1.65	…
11	F/3	Nonrecurrence	Primitive Glioma	6	50	12	1.60	1.02
12	F/20	Nonrecurrence	Germinoma	16	70	12	1.17	0.96
13	M/29	Nonrecurrence*	Malignant ganglioglioma	27	60	13	0.56	0.84
14	F/42	Nonrecurrence	Anaplastic oligoastrocytoma	13	60	19	0.40	0.61
15	M/48	Nonrecurrence	Anaplastic oligoastrocytoma	19	60	5	1.56	0.77
16	M/48	Nonrecurrence	Low-grade astrocytoma	18	60	15	1.89	0.88
17	F/19	Nonrecurrence	Malignant ganglioglioma	13	60	13	2.56	…
18	M/49	Nonrecurrence	Anaplastic oligoastrocytoma	17	60	9	1.79	…
19	F/66	Nonrecurrence	Glioblastoma	41	60	8	0.49	…
20	M/66	Nonrecurrence	Glioblastoma	35	60	22	0.84	…

*Final diagnosis was histologically proved by either surgical resection or stereotactic biopsy.

†Primitive neuroectodermal tumor.

Note.—All patients underwent systemic chemotherapy as well as radiation therapy. rCBV indicates relative cerebral blood volume.

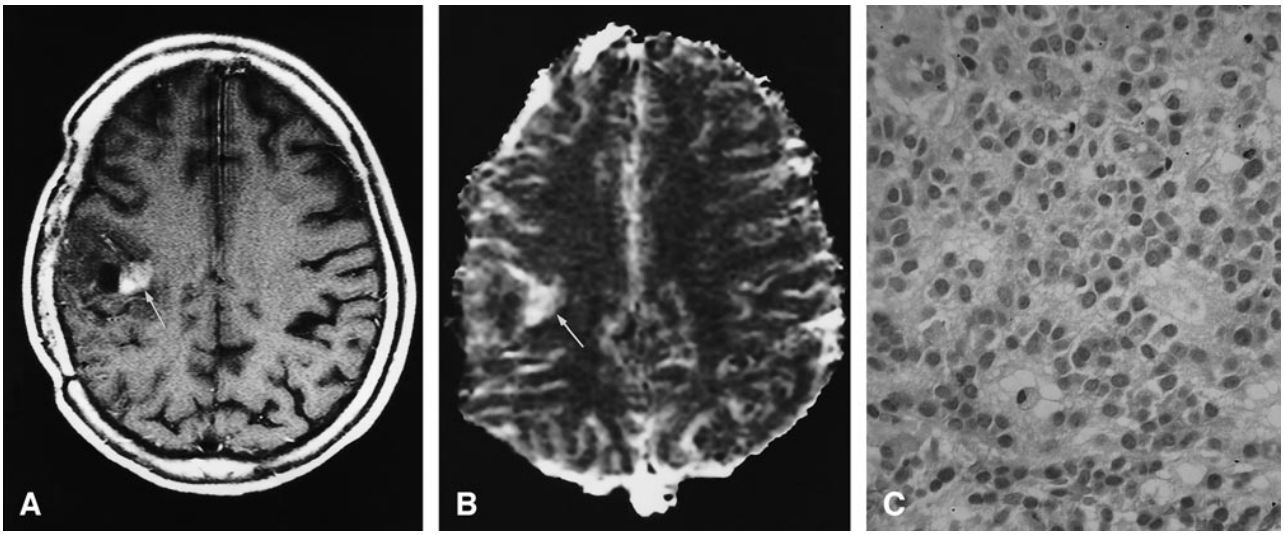

FIG 1. 63-year-old woman with a recurrent anaplastic astrocytoma verified by surgical resection.

A, Contrast-enhanced T1-weighted MR image (690/14/1; section thickness, 5 mm) shows a focally enhancing area (*arrow*) with a surrounding nonenhancing zone of low intensity and mass effect in the right frontal lobe.

B, Anaplastic astrocytoma appears as an area of hyervascularity (*arrow*) on rCBV map (normalized rCBV ratio, 4.45).

C, Histologic specimen shows densely accumulated tumor cells (hematoxylin-eosin, original magnification × 200).

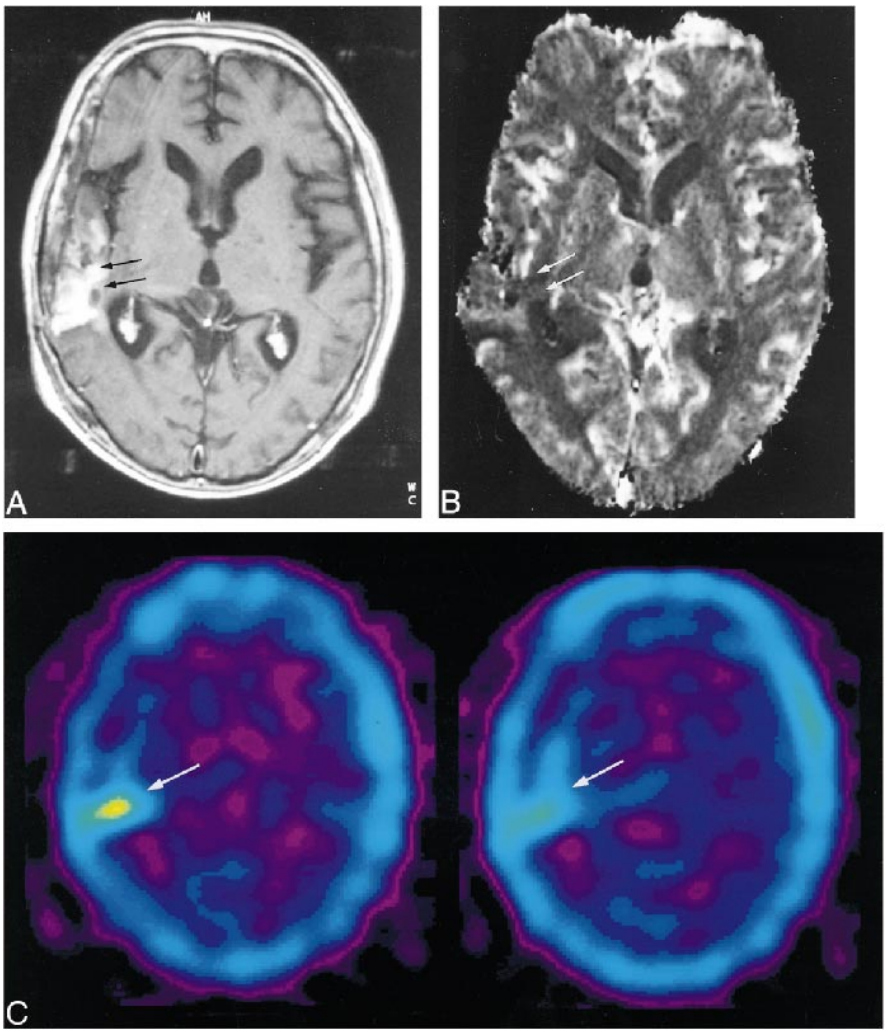

FIG 2. 78-year-old man with a recurrent glioblastoma. The diagnosis was determined by the progressively enlarging area of enhancement on serial MR images and by the patient's clinical deterioration.

A, Contrast-enhanced T1-weighted MR image (690/14/1; section thickness, 5 mm) shows inhomogeneous enhancement (*arrows*) with surrounding nonenhancing zone of low intensity and mass effect in the right temporoparietal lobe.

B, The recurrent tumor is seen as an area of hypovascularity (*arrows*) on the rCBV map (normalized rCBV ratio, 0.83).

C, ^{201}Tl-SPECT scans show abnormal uptake in the area of recurrent tumor (*arrow*), consistent with tumor recurrence.

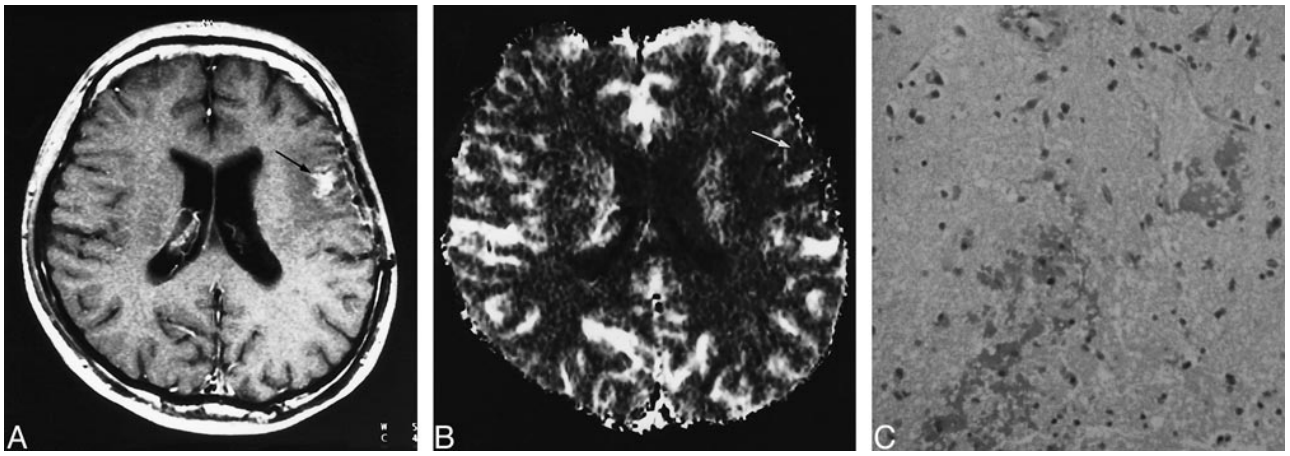

FIG 3. 29-year-old man with radiation necrosis (verified by stereotactic biopsy) who had undergone subtotal tumor resection followed by conventional radiation therapy (60 Gy) and systemic chemotherapy 26 months earlier. Ten months later, tumor recurrence was found, and was treated by subtotal resection and chemotherapy.

A, Contrast-enhanced T1-weighted MR image (690/14/1; section thickness, 5 mm) shows enhanced area (*arrow*) within surrounding nonenhancing zone of low intensity and mass effect in the left temporal lobe.

B, Radiation necrosis appears as an area of hyovascularity (*arrow*) on the rCBV map (normalized rCBV ratio, 0.56).

C, Histologic specimen shows avascular areas, consistent with radiation necrosis (hematoxylin-eosin; original magnification × 200).

FIG 4. 49-year-old man without tumor recurrence. The diagnosis was based on the decreasing size of the enhanced area on serial MR images.

A, Contrast-enhanced T1-weighted MR image (690/14/1; section thickness, 5 mm) shows a small focus of enhancement (*arrow*) within surrounding nonenhancing zone of low intensity and mass effect in the left frontal lobe.

B, Enhanced area appears as a region of hypervascularity (*arrows*) on the rCBV map (normalized rCBV ratio, 1.79).

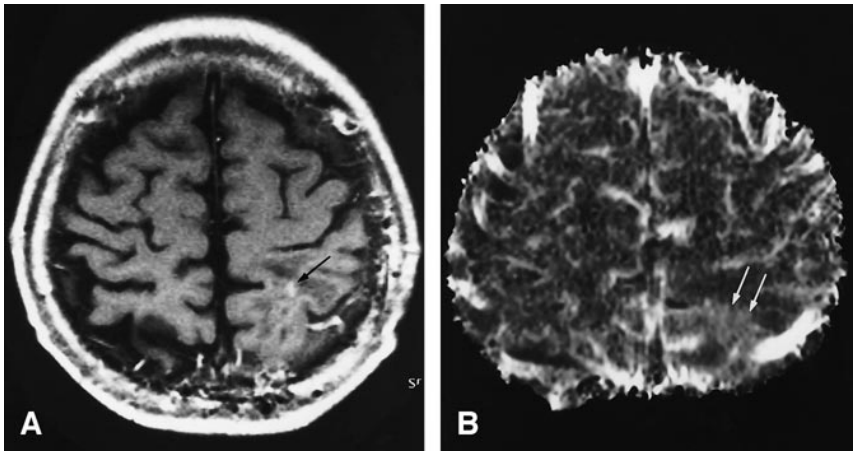

cularity, would be useful for differentiating highly vascularized recurrent tumor from avascular necrosis (18). Although the diagnosis of tumor recurrence was difficult in patients with normalized rCBV ratios of less than 2.6, diagnosis was possible by adding ^{201}Tl-SPECT studies. Several different mechanisms between the two techniques must have produced the higher sensitivity of the ^{201}Tl-SPECT examination, which will be discussed in detail in this discussion. On the basis of the results we obtained, we recommend that perfusion-sensitive contrast-enhanced MR imaging should be initially performed in patients with suspected tumor recurrence, because this study can be acquired during the same session as conventional MR imaging, and precise comparison of the findings with abnormally enhanced lesions is possible. The ^{201}Tl-SPECT examination should be added only when the diagnosis of early tumor recurrence is difficult to determine with perfusion-sensitive contrast-enhanced MR imaging. We believe that decreasing the number of patients undergoing ^{201}Tl-SPECT or positron emission tomography is important from the economic standpoint.

Overlap of the normalized rCBV ratios occurred between two groups. We speculated that this overlap might have been caused by several factors. First, the areas of recurrent tumor may not always consist of the tumor cells but may coexist with necrosis and hypovascular areas caused by occlusive vasculopathy induced by radiation. In fact, among the recurrent glioblastomas, the range of normalized rCBV ratios was from 0.83 to 3.08 (mean, 1.85), which was significantly different from the range in the initial glioblastomas we examined previously (mean, 7.32) (18). Forsyth et al (31) reported that among patients with gliomas who had previously been treated with external-beam radiotherapy and who subsequently underwent stereotactic biopsy to differentiate tumor recurrence from radiation necrosis, 33% were found to have a mixture of tumor recurrence and radiation necrosis.

Second, within irradiated brain tissues, the affected vessels do not simply consist of occlusive

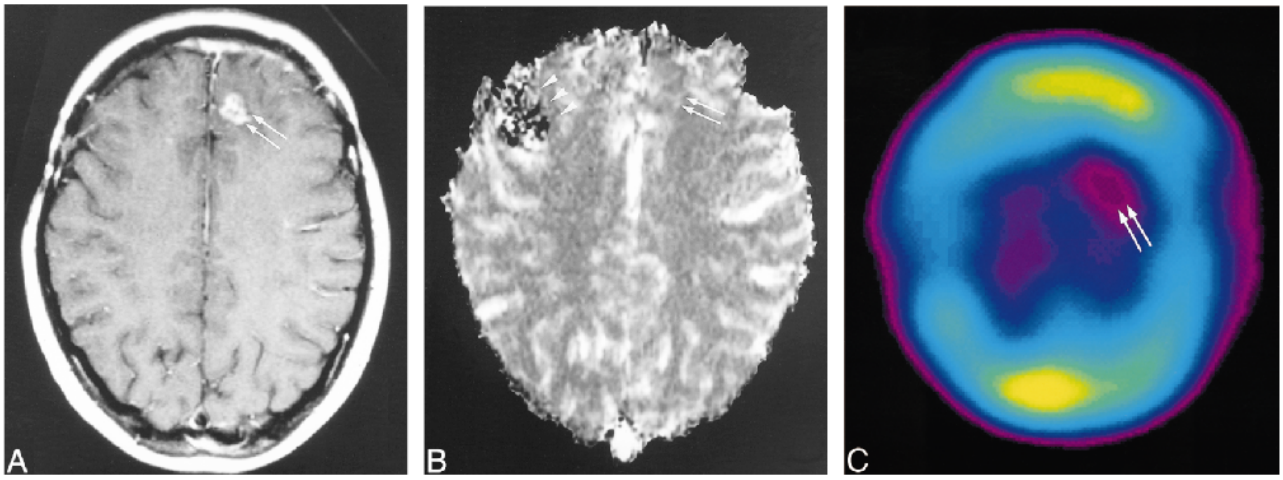

FIG 5. 20-year-old woman without tumor recurrence. The diagnosis was based on the disappearance of the enhancing area on serial MR images.

A, Contrast-enhanced T1-weighted MR image (690/14/1; section thickness, 5 mm) shows a small focus of enhancement (*arrows*) within surrounding nonenhancing zone of low intensity and mass effect in the left frontal lobe.

B, The enhancing area appears mildly hypervascular (*arrows*) on the rCBV map (normalized rCBV ratio, 1.17). The effects of previous surgery can be seen as susceptibility artifacts in right frontal region (*arrowheads*).

C, ^{201}Tl-SPECT scan shows no abnormal uptake in the enhancing lesion (*arrows*), consistent with lack of tumor recurrence.

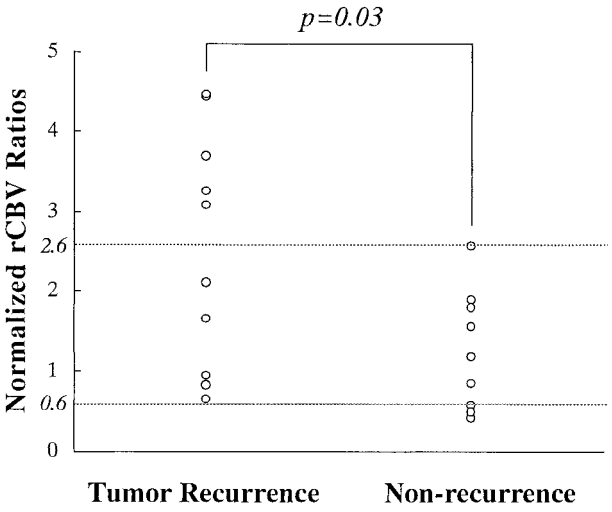

FIG 6. Relationship between normalized rCBV ratios in patients with tumor recurrence and those with nonneoplastic contrast-enhancing tissue.

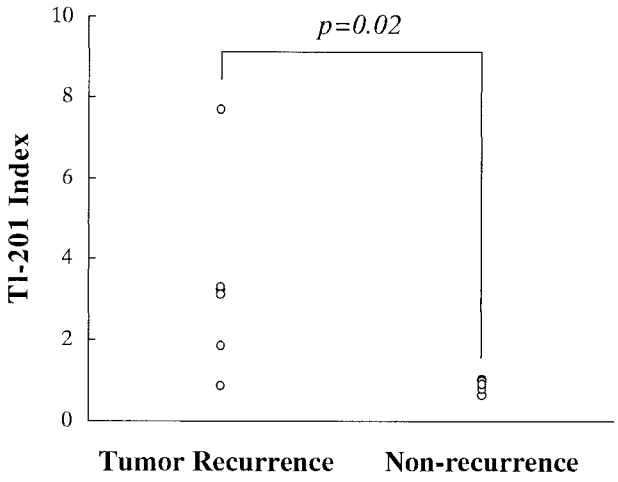

FIG 7. Relationship between thallium indexes in patients with tumor recurrence and those with nonneoplastic contrast-enhancing tissue.

vessels but rather a variety of vascular phenomena, such as aneurysmal formation, telangiectasia, vascular elongation, and a remarkable proliferation of endothelial cells, especially in the capillary bed (32, 33). Disturbance in the permeability of the capillary wall is thought to be the initial response, which causes tissue necrosis before those vessels are occluded (32, 33). In fact, in experimental studies, necrosis is frequently observed in spatial relation to capillary vessels that never undergo occlusive changes (33). Gaensler et al (34) and Okeda and Shibata (35) have hypothesized that radiation may preferentially affect the endothelium of veins, producing venoocclusive disease, with subsequent development of exudation, hemorrhage, and necrosis. These authors believe that the formation of vascular telangiectasia may represent a physiological attempt to form collateral drainage away from the area of venous occlusion and congestion. In other words, the enhanced areas might not only maintain the vascularity derived from the large vessels but also have relatively large CBV ratios because the volume of the vascular lumen increases as a result of the enlarged lumen secondary to the aneurysmal or telangiectatic formation as well as to elongated changes.

Third, petechial hemorrhage induced by radiation may produce susceptibility artifacts and decrease the normalized rCBV ratios when it occurs within areas of tumor recurrence. Although susceptibility artifacts caused by petechial hemorrhage were not visually observed within enhancing lesions in our cases, hemosiderin deposition in peri-

vascular spaces was probably present, as reported by others (34). Because we used the GE-EPI technique for perfusion-sensitive contrast-enhanced MR imaging, those artifacts might have been more prominent. The combination of these complex phenomena may make it difficult to differentiate tumor recurrence from nonneoplastic contrast-enhancing tissue.

The ^{201}Tl-SPECT studies provided useful information for detecting tumor recurrence. The accumulation of thallium, handled physiologically like potassium, is an active process and not just the result of disruption of the blood-brain barrier (36). A principal mechanism for the active uptake of thallium into viable cells is the energy-dependent Na+/K+-adenosine triphosphatase pump (37). Those processes must be maintained even within the hypovascular areas of tumor recurrence. Additionally, the difference in the thallium uptake indexes between areas of tumor recurrence and normal brain tissue must be higher than the difference in normalized rCBV ratios, because thallium never accumulates in normal brain tissue, whereas the rCBV of normal brain tissue is relatively high. Therefore, thallium indexes might be more sensitive than normalized rCBV ratios in the detection of early tumor recurrence.

We found a sensitivity of 50% and a specificity of 90% for perfusion-sensitive contrast-enhanced MR imaging when the cutoff value of the normalized rCBV ratios was 1.0. Sensitivity was 90% and specificity was 100% for ^{201}Tl-SPECT when the cutoff value of the thallium index was 1.0. To our knowledge, there has been no study of perfusion-sensitive contrast-enhanced MR imaging to determine the value of differentiation between tumor recurrence and nonrecurrence. Since the number of patients in our study was small, a more systematic evaluation is expected in the future to establish the efficacy of this technique. As with the ^{201}Tl-SPECT study, both the sensitivity and specificity obtained for the perfusion-sensitive contrast-enhanced MR imaging study were higher than those reported previously (sensitivity and specificity ranged from 67% to 94% and from 40% to 63%, respectively). Although we do not know why these figures are higher, the small number of patients may be one of the reasons (38–41).

Our study has several limitations, or pitfalls. First, the inclusion of low-grade gliomas, in which recurrent tumor would not be expected to enhance, weighted the patient population toward those cases in which posttherapeutic enhancement was unlikely to represent recurrent tumor. However, recurrent tumor usually enhances, even if the original tumor did not (42). In fact, all recurrent gliomas that were initially diagnosed as low-grade gliomas were transformed into malignant gliomas (cases 1, 3, and 9).

Second, partial voluming of the lesions may affect the rCBV data. The heterogeneity of rCBV in these lesions has previously been reported (19–26), and averaging a large ROI over the entire lesion may not provide the best information possible. Although the lesions observed in this study were small (mean, 17 mm), making it difficult to locate some ROIs within enhancing lesions in some patients, partial volume effect must be one of the important problems, and maximum rCBV ratios would have been better than normalized rCBV ratios for evaluation.

Finally, the correlation of conventional MR images, rCBV maps, and ^{201}Tl-SPECT studies may not always have been complete. For example, high rCBV areas might exist outside an enhancing lesion, as shown in Figure 2. In this case, the region more lateral to the area of enhancement seems to have increased rCBV and to correspond to the region of high thallium uptake. Although we focused on enhancing lesions in this study, evaluation of rCBV outside the enhancing lesion may be necessary in future studies.

Recently, proton MR spectroscopy, which allows in vivo measurement of the concentration of brain metabolites, such as choline-containing phospholipids, has been evaluated in regard to whether it can distinguish areas of tumor recurrence from areas of radiation effects. Preul et al (43) showed that the magnitude of the choline signal provided helpful information in distinguishing between them in diagnostically difficult cases. However, because of low spatial resolution, the differentiation may be difficult in patients with small enhancing lesions, such as those who were examined in our study.

Conclusion

When a new enhancing lesion develops within an irradiated area in a patient who was previously treated by surgery, radiotherapy, and chemotherapy for intraaxial brain tumors, it may be impossible to differentiate tumor recurrence from enhancing nonneoplastic tissue, such as radiation necrosis. Perfusion-sensitive MR imaging can offer useful information in such patients. If the normalized rCBV ratio of the enhancing lesion is more than 2.6 or less than 0.6, tumor recurrence or radiation necrosis should be strongly suspected, and we think it is not necessary to perform ^{201}Tl-SPECT. If the enhancing lesion has a normalized rCBV ratio between 0.6 and 2.6, ^{201}Tl-SPECT may be useful. Perfusion-sensitive MR imaging can easily be added to a routine MR examination, and may help decrease the number of patients undergoing ^{201}Tl-SPECT examination.

References

1. Tsuruda JS, Kortman KE, Bradley WG, Wheeler DC, Dalsem WV, Bradley TP. **Radiation effects on cerebral white matter: MR evaluation.** *AJR Am J Roentgenol* 1987;149:165–171
2. Remler MP, Marcussen WH, Tiller-Borsich J. **The late effects of radiation on the blood brain barrier.** *Int J Radiat Oncol Biol Phys* 1986;12:1965–1969

3. Dooms GC, Hecht S, Brant-Zawadzki M, Berthiaume Y, Norman D, Newton TH. **Brain radiation lesions: MR imaging.** *Radiology* 1986;158:149–155
4. Nishimura R, Takahashi T, Morishita S, Sumi M, Uozumi H, Sakamoto Y. **MR Gd-DTPA enhancement of radiation injury.** *Radiat Med* 1992;10:101–108
5. Kim EE, Chung SK, Haynie TP, et al. **Differentiation of residual or recurrent tumors from post-treatment changes with F-18 FDG PET.** *Radiographics* 1992;12:269–279
6. Rosen BR, Aronen HJ, Kwong KK, Belliveau JW, Hamberg LM, Fordbam JA. **Advances in clinical neuroimaging functional MR imaging techniques.** *Radiographics* 1993;13:889–896
7. Aronen, HJ, Gazit IE, Luis DN, et al. **Cerebral blood volume maps of gliomas: comparison with tumor grade and histologic findings.** *Radiology* 1994;191:41–51
8. Maeda M, Itoh S, Kimura H, et al. **Tumor vascularity in the brain: evaluation with dynamic susceptibility-contrast MR imaging.** *Radiology* 1993;189:233–238
9. Wenz F, Rempp K, Hess T, et al. **Effect of radiation on blood volume in low-grade astrocytomas and normal brain tissue: quantification with dynamic susceptibility contrast MR imaging.** *AJR Am J Roentgenol* 1996;166:187–193
10. Bruening R, Kwong KK, Vevea MJ, et al. **Echo-planar MR determination of relative cerebral blood volume in human brain tumors: T1 versus T2 weighting.** *AJNR Am J Neuroradiol* 1996; 17:831–840
11. Rabin BM, Meyer JR, Berlin JW, Marymount MH, Palka PS, Russell EJ. **Radiation-induced changes in the central nervous system and head and neck.** *Radiographics* 1996;16:1055–1072
12. Ricci PE, Karis JP, Heiserman JE, Fram EK, Bice AN, Drayer BP. **Differentiating recurrent tumor from radiation necrosis: time for re-evaluation of positron emission tomography?** *AJNR Am J Neuroradiol* 1998;19:407–413
13. Weisskoff R, Belliveau J, Kwong K, Rosen B. **Functional MR imaging of capillary hemodynamics.** In: Potchen E, ed. *Magnetic Resonance Angiography: Concepts and Applications.* St Louis: Mosby;1992;14:538–546
14. Villringer A, Rosen BR, Belliveau JW, et al. **Dynamic imaging with lanthanide chelates in normal brain: contrast due to magnetic susceptibility effects.** *Magn Reson Med* 1988;6:164–174
15. Majumdar S, Gore JC. **Studies of diffusion in random fields produced by variations in susceptibility.** *J Magn Reson* 1988; 78:41–51
16. Axel L. **Cerebral blood flow determination by rapid-sequence computed tomography: a theoretical analysis.** *Radiology* 1980; 137:679–686
17. Rosen BR, Belliveau JW, Chien D. **Perfusion imaging nuclear magnetic resonance.** *J Magn Reson Q* 1989;5:263–281
18. Sugahara T, Korogi Y, Kochi M, et al. **Relationship of MR determined cerebral blood volume maps to histologic and angiographic vascularities of gliomas.** *AJR Am J Roentgenol* 1998; 171:1479–1486
19. Caveness WF. **Pathology of radiation damage to the normal brain of the monkey.** *Natl Cancer Inst Monogr* 1977;46:57–76
20. Yoshii Y, Phillips TL. **Late vascular effects of whole brain X-irradiation in the mouse.** *Acta Neurochir* 1982;64:87–102
21. Gutin PH, Leibel SA, Sheline GE, et al. ***Radiation Injury to the Nervous System.*** New York: Raven; 1991
22. Valk PE, Dillon WP. **Radiation injury of the brain.** *AJNR Am J Neuroradiol* 1991;12:45–62
23. Curran WJ, Hecht-Leavitt C, Schut L, Zimmerman RA, Nelson DF. **Magnetic resonance imaging of cranial radiation lesions.** *Int J Radiat Oncol Biol Phys* 1987;13:1093–1098
24. Grossman RI, Hecht-Leavitt CM, Evans SM, et al. **Experimental radiation injury: combined MR imaging and spectroscopy.** *Radiology* 1988;169:305–309
25. Lundqvist H, Rosander K, Lomanov M, et al. **Permeability of the blood-brain barrier in the rat after local proton irradiation.** *Acta Radiol Oncol* 1982;21:267–271
26. Miot E, Hoffschir D, Alapettie C, et al. **Experimental MR study of cerebral radiation injury: quantitative T2 changes over time and histopathologic correlation.** *AJNR Am J Neuroradiol* 1995; 16:79–85
27. Reinhold HS, Endrich B. **Tumor microcirculation as a target for hyperthermia: review.** *Int J Hyperthermia* 1986;2:111–137
28. Song CW, Lokshina A, Rhee JG, Patten M, Levitt SH. **Implication of blood flow in hyperthermic treatment of tumors.** *IEEE Trans Biomed Eng* 1984;31:9–16
29. Scatliff JH, Guinto FC Jr. **Vascular patterns in cerebral neoplasms and their differential diagnosis.** *Semin Roentgenol* 1971; 6:59–69
30. Scatliff JH, Radcliffe WB, Pittman HH, Park CH. **Vascular structure of glioblastomas.** *AJR Am J Roentgenol* 1969;105:795–805
31. Forsyth PA, Kelly PJ, Cascino TL, Scheithauer BW, et al. **Radiation necrosis or glioma recurrence: is computer-assisted stereotactic biopsy useful?** *J Neurosurg* 1995;82:436–444
32. Di Chiro G, Oldfield E, Wright DC, et al. **Cerebral necrosis after radiotherapy and/or intraarterial chemotherapy for brain tumors: PET and neuropathologic studies.** *AJR Am J Roentgenol* 1988;150:189–197
33. Haymaker W, Ibrahim MZ, Miquel J, Call N., Riopelle AJ. **Delayed radiation effects in the brains of monkeys exposed to X- and g-rays.** *J Neuropathol Exp Neurol* 1968;27:50–79
34. Gaensler EHL, Dillon WP, Edwards MSB, Larson DA, Rosenau W, Wilson CB. **Radiation-induced telangiectasia in the brain simulates cryptic vascular malformations at MR imaging.** *Radiology* 1994;193:629–636
35. Okeda R, Shibata T. **Radiation encephalopathy: an autopsy case and some comments on the pathogenesis of delayed radionecrosis of the central nervous system.** *Acta Pathol Jpn* 1973;23: 867–883
36. Kaplan WD, Takvorian T, Morris JH, Rumbaugh CL, Connolly BT, Atkins HL. **Thallium 201 brain tumor imaging: a comparative study with pathologic correlation.** *J Nucl Med* 1987;28: 47–52
37. Brismar T, Collins VP, Kesselberg M. **Thallium-201 uptake relates to membrane potential and potassium permeability in human glioma cells.** *Brain Res* 1989;500:30–36
38. Kahn D, Follett KA, Nathan MA, Piper JG, Madsen M, Kirchner PT. **Diagnosis of recurrent brain tumor: value of 201-Tl SPECT vs 18-F-fluorodeoxyglucose PET.** *AJR Am J Roentgenol* 1994;163:1459–1465
39. Kline JL, Noto RB, Glantz M. **Single-photon emission CT in the evaluation of recurrent brain tumor in patients treated with gamma knife radiosurgery or conventional radiation therapy.** *AJNR Am J Neuroradiol* 1996;17:1681–1686
40. Yoshii Y, Satou M, Yamamoto T, et al. **The role of thallium-201 single photon emission tomography in the investigation and characterization of brain tumor in man and their response to treatment.** *Eur J Nucl Med* 1993;2:39–45
41. Moustafa HM, Omar WM, Ezzat I, Ziada GA, Ghonimy EG. **201-Tl single photon emission tomography in the evaluation of residual and recurrent astrocytoma.** *Nucl Med Commun* 1994;15: 140–143
42. WS Atlas,Lavi E. **Intra-axial brain tumors.** In: Atlas SW, ed. *Magnetic Resonance Imaging of the Brain and Spine.* 2nd ed. Philadelphia: Lippincott-Raven;1996;10:415–417
43. Preul MC, Leblanc R, Caramanos Z, Kasrai R, Arnold DL. **Magnetic resonance spectroscopy guided brain tumor resection: differentiation between recurrent glioma and radiation change in two diagnostically difficult cases.** *Can J Neurol Sci* 1998;25: 13–22